Bulk and Surface Structures of the Aurivillius Phases: $Bi_{4-x}La_xTi_3O_{12}$ ($0 \leq x \leq 2.00$)

Ming-Wen Chu,† Maria-Teresa Caldes, Luc Brohan, Marcel Ganne, Anne-Marie Marie, Olivier Joubert, and Yves Piffard*

Institut des Matériaux Jean Rouxel, UMR CNRS, Université de Nantes No. 6502, 2 rue de la Houssinière, BP 32229 44322 Nantes Cedex 3, France

Received May 26, 2003. Revised Manuscript Received October 20, 2003

A convergent beam electron diffraction (CBED) study of $Bi_2La_2Ti_3O_{12}$ was performed. As in the case of $Bi_3LaTi_3O_{12}$, it reveals a *lowering of symmetry* with respect to the idealized structure (space group *I*4/*mmm*) of Aurivillius phases. The structure of $Bi_{4-x}La_xTi_3O_{12}$ (x = 1 and 2) compounds has been refined from powder X-ray diffraction data, showing that the interlayer mismatch between fluorite-like and perovskite-like layers is relieved by the conjuction of *cation disorder* and *lowering of symmetry*. HREM studies performed on $Bi_{4-x}La_xTi_3O_{12}$ (x = 0, 0.75, and 2) compounds show that the La-containing compounds exhibit intergrowth defects within a thickness of ∼5 nm from the crystal surface to bulk. Taking into account both the enrichment of the surface with La and Bi, and the preference of La^{3+} for a 12-fold coordination, a model is proposed for the formation of such defects. They correspond to the growth of A-site cation-deficient perovskite compounds, $(Bi,La)_{3.33}Bi_2Ti_2O_{12}$ and $(Bi,La)_{3.66}Bi_3TiO_{12}$.

1. Introduction

The structure of Aurivillius phases can be described as the intergrowth of fluorite-like $[M_2O_2]^{2+}$ units and perovskite-like $[A_{n-1}B_nO_{3n+1}]^{2-}$ slabs, where $n = 1-5$.[1] The 12-fold perovskite A sites can be occupied by cations such as Ba^{2+}, Ca^{2+}, Sr^{2+}, Bi^{3+}, and the rare earth cations, and the 6-fold B sites can be occupied by cations such as Ti^{4+}, Ta^{5+}, Nb^{5+} and W^{6+}, leading to BO_6 octahedra.[2]

The idealized structure (space group (SG) *I*4/*mmm*, No. 139) of the $n = 3$ Aurivillius compound $Bi_4Ti_3O_{12}$ (BTO) is shown in Figure 1. However, the actual crystal structure of BTO, determined by Rae et al.[3] from single-crystal X-ray diffraction data, exhibits a small displacive perturbation away from this idealized model. It corresponds in fact to a commensurate modulation ($q = b^*$) of an orthorhombic average structure (SG *Fmmm*, No. 69), leading to the monoclinic SG *B1a1* (nonstandard setting of *P1c1*, No. 7) with a = 5.450(1) Å, b = 5.4059(6) Å, c = 32.832(1) Å, and β = 90°. Most of the Aurivillius phases reported to date exhibit a rather similar distortion associated with the interlayer mismatch between fluorite-like $[M_2O_2]^{2+}$ units and perovskite-like slabs.[4] The monoclinic distortion of BTO predominantly arises from the octahedral tilting,[3,5] which

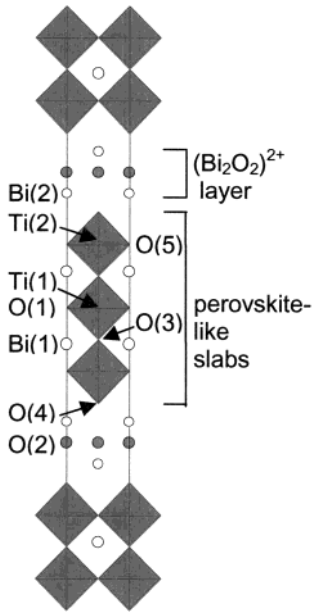

Figure 1. [100] view of the idealized (SG *I*4/*mmm*) structure of the $n = 3$ Aurivillius phase $Bi_4Ti_3O_{12}$.

reduces the *ab*-plane size of perovskite-like slabs, thus resulting in the relief of mismatch strain. In addition, this interlayer mismatch also plays an important role in the stability of Aurivillius phases.[4]

In Aurivillius phases, the substitution of cations with proper ionic radii was also believed to be a mismatch relief mechanism.[4,6] In an early study of rare earth bismuth titanates, $Bi_{4-x}Ln_xTi_3O_{12}$ (Ln = La, Pr, Nd, and

* To whom correspondence should be addressed. E-mail: piffard@cnrs-imn.fr.
† Present address: Max-Planck-Institut für Mikrostrukturphysik, Weinberg 2, D-06120, Halle (Saale), Germany.

(1) Aurivillius, B. *Ark. Kemi* **1949**, *1*, 499.
(2) Hervoches, C. H.; Lightfoot, P. *J. Solid State Chem.* **2000**, *153*, 66.
(3) Rae, A. D.; Thompson, J. G.; Withers, R. L.; Willis, A. C. *Acta Crystallogr.* **1990**, *B46*, 474.
(4) Armstrong, R. A.; Newnham, R. E. *Mater. Res. Bull.* **1972**, *7*, 1025.
(5) Hervoches, C. H.; Lightfoot, P. *Chem. Mater.* **1999**, *11*, 3359.
(6) Wolfe, R. W.; Newnham, R. E. *J. Electrochem. Soc.* **1969**, *116*, 832.

10.1021/cm030341m CCC: $27.50
Published on Web 12/09/2003

Sm−Lu), Wolfe et al. have indicated that rare earth cations substitute for Bi^{3+} at the 12-fold A site of perovskite-like slabs exclusively (i.e., that Ln/Bi combinations cannot occupy the 8-fold Bi site of the $[Bi_2O_2]^{2+}$ layers).[6] However, recent structural refinements of $n = 1$, 2, and 3 Aurivillius structures indicate that the M site can be occupied by Pb^{2+}, [7,8] and also by cations without lone pair, such as Ba^{2+}, Sr^{2+}, Ca^{2+}, and La^{3+}. [2,9,10] Therefore, a partial cation mixing can occur at M and A sites, which is referred to as the *cation disorder*.[2,7−11]

In a recent X-ray and neutron powder diffraction study of $Bi_{4-x}La_xTi_3O_{12}$ ($x = 1$ and 2) [2], both structures were analyzed in the centrosymmetric SG *I*4/*mmm* coupled with the distribution of Bi^{3+}/La^{3+} over the M/A sites. This *cation disorder*, which increases when x increases, was suggested to be a second type of mechanism for the relief of mismatch strain, since the octahedral distortion is absent for SG *I*4/*mmm* [2]. However, this space group is not compatible with the ferroelectricity of $Bi_3LaTi_3O_{12}$ (BLT1.00) thin films capacitors,[12] and evidence for a monoclinic distortion, similar to that of BTO, has recently been obtained for this compound from a convergent beam electron diffraction (CBED) study.[13] Therefore, the inherent strain present in BLT1.00 is in fact relieved by the conjunction of *cation disorder* and *lowering of symmetry*. On account of this, the crystal structure of this compound was reexamined from a Rietveld analysis of powder X-ray diffraction data, and the results are presented in the first part of this paper. Concerning $Bi_2La_2Ti_3O_{12}$ (BLT2.00), the structural study mentioned above [2] shows that the *cation disorder* is much more pronounced in BLT2.00 than in BLT1.00. Therefore, because ferroelectricity was not observed in BLT2.00,[14] the actual SG could be *I*4/*mmm* and in that case the *cation disorder* would be, on its own, a mechanism for the relief of mismatch strain. To verify this the BLT2.00 phase was analyzed using selected area electron diffraction (SAED) and CBED techniques and its crystal structure was reexamined from a Rietveld analysis of powder X-ray diffraction data.

An X-ray photoelectron spectroscopy (XPS) study of $Bi_{4-x}La_xTi_3O_{12}$ ($x = 0.50$, 0.75, 1.00, 1.50, and 2.00) solid solution members was recently performed.[15] For all samples, it was shown that the chemical composition of the surface is quite different from that of the bulk, with a significant excess in bismuth and a slight enrichment with lanthanum, while titanium always exhibits a considerable deficiency. From a subsequent high-resolution electron microscopy (HREM) study of $Bi_{3.25}La_{0.75}Ti_3O_{12}$ (BLT0.75) it was suggested that this surface nonstoichiometry arises from intergrowth defects consisting of rock-salt-like $[(Bi,La)O]_2$ layer(s) and perovskite block(s) at the crystal edge,[15] instead of the regular stacking of fluorite-like $[Bi_2O_2]^{2+}$ units and perovskite-like slabs of Aurivillius phases. It was explained that the surface excess La^{3+} tends to occupy the cation site in the $[M_2O_2]^{2+}$ layer, but because La^{3+} prefers a more symmetrical environment than Bi^{3+}, this induces a structural change of this layer from fluorite-like to rock-salt-like.[15] However, Boullay et al. [16]recently reported that Aurivillius phases can be described as cation-deficient perovskites with a general formula of $AB_{1-x}O_3$, i.e., as the stacking of $AO-\square O_2-AO-BO_2$ idealized planes along a ⟨001⟩ direction of the ideal cubic perovskite cell (where AO is a rock-salt-like plane, i.e., square array of alternating A and O atoms; and BO_2 is a perovskite-type plane, i.e., equatorial plane of corner-sharing BO_6 octahedra). This model significantly simplifies the structural complexity of Aurivillius compounds and makes the mismatch between the fluorite-like layers and perovskite-like slabs [2,3,5] much easier to understand.[16] In addition, it reveals that the descriptions concerning the rock-salt-like $[(Bi,La)O]_2$ layer(s) of intergrowth defects at the crystal edge of BLT0.75 are likely inadequate.[15] Consequently, to clarify this latter point in the light of Boullay et al.'s model, a HREM study was performed on $Bi_{4-x}La_xTi_3O_{12}$ ($x = 0$, 0.75, and 2.00) phases.

2. Experimental Section

The $Bi_{4-x}La_xTi_3O_{12}$ ($x = 0$, 0.75, 1.00, and 2.00) powder compounds were prepared via the Pechini method, as reported previously.[13,15]

X-ray diffraction (XRD) patterns of these compounds were collected at room temperature in a Debye−Scherrer geometry using an INEL 120 curved position sensitive detector, equipped with a quartz monochromator (Cu $K\alpha_1$ radiation; $\lambda = 1.540598$ Å). To minimize the strong absorption of bismuth and lanthanum, powders were glued around the Lindemann capillary of 0.1-mm diam. This procedure was proved to be effective in dealing with absorbing compounds.[17,18] Such XRD data were recorded in the range of $10° < 2\theta < 120°$ with a total acquisition time of ∼18 h. The structure refinement was carried out by the Rietveld method using the RIETICA program.[19]

Powder samples of the $Bi_{4-x}La_xTi_3O_{12}$ ($x = 0$, 0.75, and 2.00) compounds were ground in butanol. A carbon-coated Cu grid was used to collect the microcrystals which were used for SAED and CBED studies performed on a Philips CM30 electron microscope operating at 300 kV, and for the HREM studies carried out with a Hitachi H9000NAR electron microscope operating at 300 kV with a Scherzer resolution of 1.8 Å. HREM image simulations were performed with the MacTempas[20] program using the multi-slice method.

3. Results and Discussion

3.1. Electron Diffraction Study. The 3D reconstruction of the reciprocal lattice of BLT2.00 was

(7) Rentschler, T. *Mater. Res. Bull.* 1997, *32*, 351.
(8) Millan, P.; Castro, A.; Torrance, J. B. *Mater. Res. Bull.* **1993**, *28*, 117.
(9) Blake, S. M.; Falconer, M. J.; McCreedy, M.; Lightfoot, P. *J. Mater. Chem.* **1997**, *7*, 1609.
(10) Ismunander; Kennedy, B. J. *J. Mater. Chem.* **1999**, *9*, 541.
(11) Vannier, R. N.; Mairesse, G.; Abraham, F.; Nowogrocki, G. *Solid State Ionics* **1994**, *70/71*, 248.
(12) Wu, D.; Li, A.; Zhu, T.; Li, Z.; Liu, Z.; Ming, N. *J. Mater. Res.* **2001**, *16*, 1325.
(13) Chu, M.-W.; Caldes, M. T.; Piffard, Y.; Marie, A.-M.; Gautier, E.; Joubert, O.; Ganne, M.; Brohan, L. *J. Solid State Chem.* **2003**, *172*, 389.
(14) Takenaka, T.; Sakata, K. *Ferroelectrics* **1981**, *38*, 769.
(15) Chu, M.-W.; Ganne, M.; Caldes, M. T.; Brohan, L. *J. Appl. Phys.* **2002**, *91*, 3178.
(16) Boullay, Ph.; Trolliard, G.; Mercurio, D.; Perez-Mato, J. M.; Elcoro, L. *J. Solid State Chem.* **2002**, *164*, 252. Boullay, Ph.; Trolliard, G.; Mercurio, D.; Perez-Mato, J. M.; Elcoro, L. *J. Solid State Chem.* **2002**, *164*, 261.
(17) Jouanneaux, A.; Joubert, O.; Evain, M.; Ganne, M. *Powder Diffr.* **1992**, *7*, 206.
(18) Joubert, O.; Jouanneaux, A.; Ganne, M. *Mater. Sci. Forum* **1993**, *133*, 795.
(19) Hunter, B. *LHPM-Rietica Rietveld*,; ANSTO: Australia, 2000.
(20) MacTempas, V 1.70, Pear Kilaas; Total Resolution: Berkeley, CA.

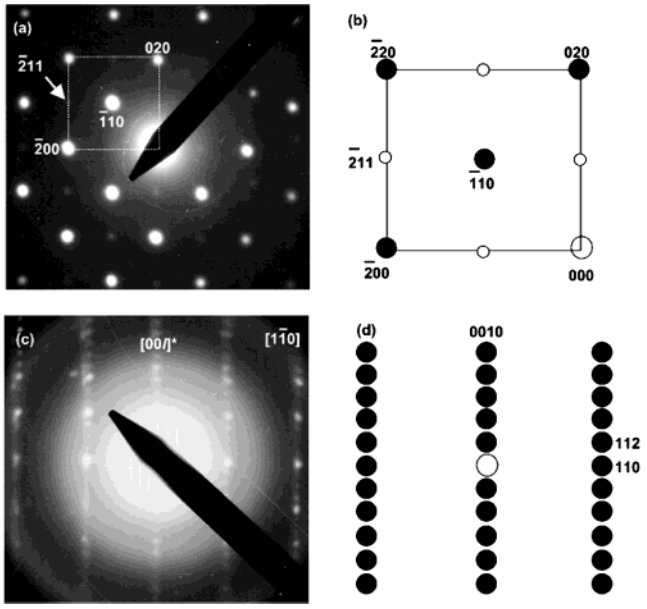

Figure 2. SAED patterns of $Bi_2La_2Ti_3O_{12}$: (a) along the [001] zone axis; (b) schematic representation of the pattern delimited by a white square; (c) [1$\bar{1}$0] zone axis; and (d) schematic pattern corresponding to (c).

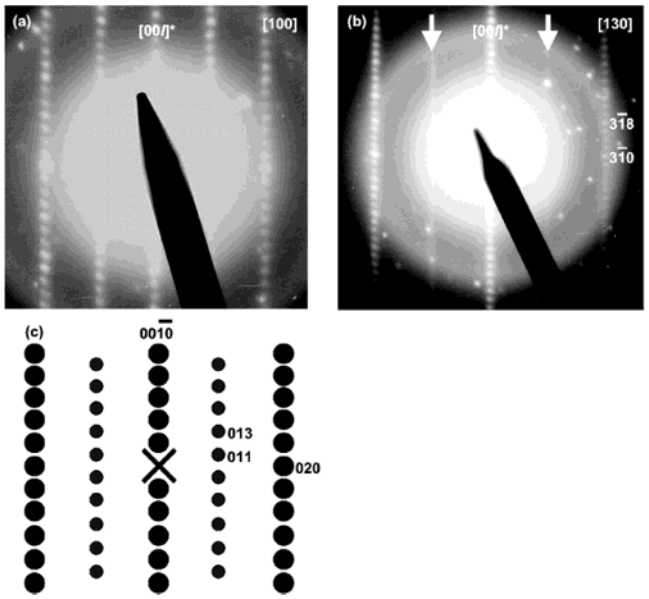

Figure 3. SAED patterns of $Bi_2La_2Ti_3O_{12}$ along (a) [100] and (b) [130] zone axes; (c) schematic pattern corresponding to (a).

performed from SAED patterns. They are shown in Figure 2 ([001] and [1$\bar{1}$0] zone axis patterns (ZAPs)) and Figure 3 ([100] and [130] ZAPs). All reflections can be indexed with a tetragonal lattice ($a = b \approx 3.8$ Å and $c \approx 33$ Å). The existence conditions (hkl: $h + k + l = 2n$; $hk0$: $h + k = 2n$; $0kl$: $k + l = 2n$; and hhl: $l = 2n$) suggest that BLT2.00 crystallizes in the tetragonal SG $I4/mmm$ (No. 139). However, diffuse "lines" are always present in the [130] ZAP (see the white arrows in Figure 3b). Note that no reflection in this pair of diffuse "lines" can be explained by the tetragonal symmetry, which refers to the possible existence of an orthorhombic distortion. To examine this hypothesis, a CBED study was performed.

Figure 4a shows the whole pattern (WP) of the [001] ZAP. At first sight, two sets of mirror planes intersecting

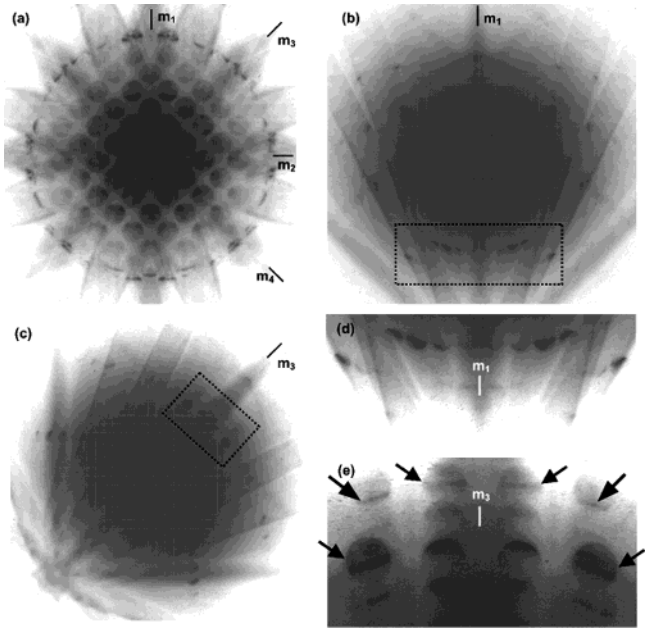

Figure 4. CBED patterns of $Bi_2La_2Ti_3O_{12}$: (a) whole pattern (WP) of the [001] zone axis; (b) and (c) HOLZ patterns tilting along m_1 and m_3, i.e., [010]* and [110]* directions, respectively; (d) and (e) enlarged patterns of the zones indicated by dashed boxes in (b) and (c), respectively.

practically with an angle of 45° can be observed, i.e., m_1 and m_2, and m_3 and m_4, respectively. In addition, the first-order Laüe zone (FOLZ) reflections appear as a ring surrounding disks in the zero order Laüe zone (ZOLZ). A further investigation concerning the intensity distribution of excess lines in FOLZ reflections and the position of diffracted disks, indicates, however, that only two mirror planes (m_1 and m_2) might exist. Therefore, the WP symmetry should be $2mm$. To confirm this assignment, the inspection of the 3D information is crucial, and the crystal was thus tilted successively along [010]* (m_1: Figure 4b) and [110]* (m_3: Figure 4c), so as to obtain FOLZ and higher order Laue zone (HOLZ) reflections. The HOLZ reflections along [010]*, displayed on an expanded scale (Figure 4d), exhibit a mirror symmetry. This suggests that the set of m_1 and m_2 mirror planes does exist. In contrast, as slight differences can be observed in the intensity distribution of HOLZ reflections along [110]* (see the black arrows in Figure 4e) the existence of m_3 and m_4 mirror planes is ruled out. Consequently, this 3D information indicates that the WP symmetry belongs to $2mm$. These characteristics are compatible with the diffraction groups $2mm$ and $2mm1_R$, which correspond to the orthorhombic point groups $mm2$ and mmm, respectively, according to Tables 1 and 2 (after Buxton et al. [21,22]). Therefore, the actual symmetry of BLT2.00 is orthorhombic rather than tetragonal.

Analogous to monoclinic BLT1.00, BLT2.00 also exhibits a *lowering of symmetry* with respect to the idealized SG $I4/mmm$, which suggests that the mismatch strain in BLT2.00 is still significant enough to induce a structural distortion. However, one can quali-

(21) Buxton, B. F.; Eades, J. A.; Steeds, J. W.; Rackham, G. M. *Philos. Trans. R. Soc.* **1976**, *281*, 181.
(22) Williams, D. B.; Carter, C. B. *Transmission Electron Microscopy*; Plenum Press: New York, 1996; Vol. II, pp 331−334.

Table 1. CBED Pattern Symmetries[a]

whole pattern	bright field	diffraction group
m	*m*	*m*
m	*m*	$2_R mm_R$
2*mm*	2*mm*	2*mm*
2*mm*	2*mm*	$2mm1_R$

[a]From Buxton et al., refs 21 and 22.

Table 2. Zone-Axis Symmetries[a]

orthorhombic		tetragonal	
point group	[001]	point group	[001]
mmm	$2mm1_R$	4/*mmm*	$4mm1_R$
*mm*2	2*mm*	−42*m*	$4_R mm_R$
222	$2m_R m_R$	4*mm*	4*mm*
		422	$4m_R m_R$

[a]From Buxton et al., refs 21 and 22.

tatively propose that the mismatch decreases with the increase in La^{3+} substitution rate, as the *lowering of symmetry* from tetragonal to orthorhombic is sufficient for BLT2.00.

3.2 X-ray Diffraction Study. As already mentioned above, the structures of BLT1.00 and BLT2.00 were previously analyzed in the centrosymmetric SG *I*4/*mmm*, but this study only reported the refined occupancies of the M/A sites by Bi^{3+}/La^{3+}, i.e., an evaluation of the *cation disorder*.[2] Therefore, since it has now been demonstrated that both compounds exhibit a *lowering of symmetry* (monoclinic for BLT1.00[13] and orthorhombic for BLT2.00), their structure was reexamined, although we knew that the X-ray scattering is dominated by Bi and La, and therefore that the precision of oxygen atoms from X-ray refinements of powder data is usually poor.

3.2.1 BLT1.00. In the refinement of cell parameters by full pattern matching no deviation from metric orthorhombic symmetry could be observed for BLT1.00 (This is also true for BLT0.75: $a = 5.4181(6)$ Å, $b = 5.4168(3)$ Å, $c = 32.8856(4)$ Å). Consequently, there is an intrinsic impossibility to perform a Rietveld analysis that would enable describing the monoclinic distortion. In addition, all diffraction peaks were perfectly interpreted with SG *B*2*cb* (nonstandard setting of *Aba*2, No. 41), which means that the weak *hk*0 reflections ($h = 2n$, $k = 2n + 1$, observed by SAED[13]) which preclude the b-glide plane are too weak to be observed by powder XRD. Therefore, a description of the structure with SG *B*2*cm* is also precluded. The room-temperature neutron powder diffraction pattern of BTO was recently analyzed similarly,[5] and a satisfactory refinement of the structure was achieved with the orthorhombic *B*2*cb* model (this structure is displayed in Figure 5). Consequently, the crystallographic data of BTO in *B*2*cb* was taken as the starting model for the Rietveld analysis of BLT1.00, coupled with the appropriate occupancy of La^{3+} in the perovskite-like slabs.

To obtain a stable refinement, several constraints were introduced: (a) The isotropic atomic displacement parameters (ADPs) of oxygen atoms were all fixed at a reasonable value, 1.2 Å^2. (b) The isotropic ADPs and atomic positions of A-site cations (i.e., Bi(1) and La(1)), and those of Bi^{3+}/La^{3+} in the $[M_2O_2]^{2+}$ layer (i.e., Bi(2) and La(2)), were constrained to be equivalent, although we knew the clear preference of La^{3+} for a more symmetrical environment than Bi^{3+}. This induces an increase in both ADPs and ESDs of the corresponding positional parameters. (c) The isotropic ADPs of the 6-fold B sites (i.e., Ti(1) and Ti(2)) were also considered as equal.

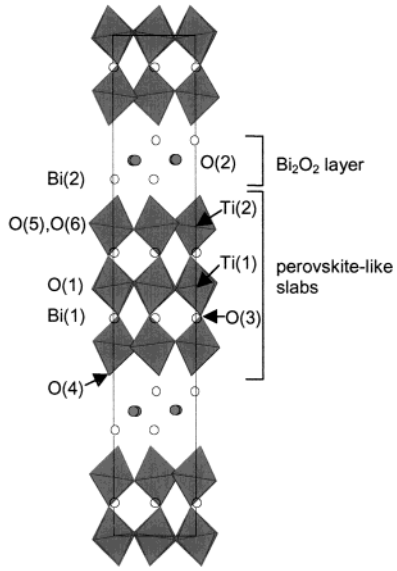

Figure 5. [100] View of the $Bi_4Ti_3O_{12}$ structure using the *B*2*cb* model.

Table 3. Positional and Thermal Parameters for $Bi_3LaTi_3O_{12}$′

atom	Wyckoff position	*x*	*y*	*z*	B_{iso}(Å^2)	occ.
Bi(1)	8b	0[b]	−0.0080(9)	0.0676(5)	1.62(2)	0.517(2)
La(1)	8b	0[b]	−0.0080(9)	0.0676(5)	1.62(2)	0.483(2)
Bi(2)	8b	−0.0018(8)	0.0165(4)	0.2111(9)	1.57(5)	0.983(2)
La(2)	8b	−0.0018(8)	0.0165(4)	0.2111(9)	1.57(5)	0.017(2)
Ti(1)	4a	0.4804(6)	0	0	0.57(6)	1
Ti(2)	8b	−0.0134(9)	0.9999(2)	0.3703(3)	0.57(6)	1
O(1)	8b	0.2156(2)	0.1879(8)	0.0043(9)	1.2	1
O(2)	8b	0.2432(5)	0.1938(9)	0.2452(6)	1.2	1
O(3)	8b	−0.0242(5)	0.0410(5)	0.4406(2)	1.2	1
O(4)	8b	−0.0189(1)	0.9729(9)	0.3190(5)	1.2	1
O(5)	8b	0.2389(8)	0.2261(7)	0.1129(3)	1.2	1
O(6)	8b	0.2486(6)	0.2188(9)	0.8785(6)	1.2	1

[a] SG *B*2*Cb*; $a = 5.4164(2)$ Å, $b = 5.4157(3)$ Å, $c = 32.9133(2)$ Å; no. of reflections = 272. R_p(%) = 3.4; R_{wp}(%) = 4.7; $\chi 2 = 9.4$. [b] Fixed coordinate to define the origin.

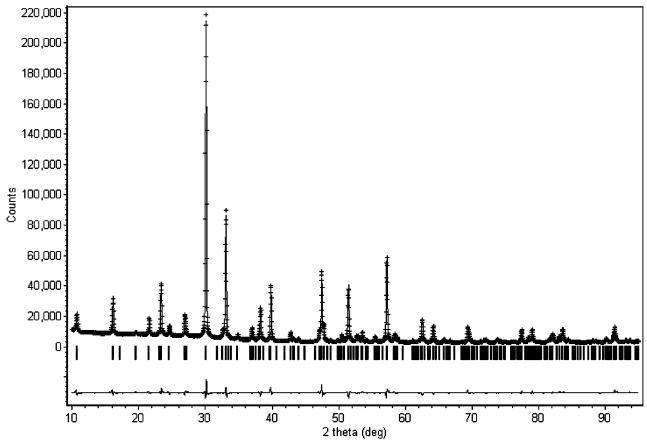

Figure 6. XRD pattern of $Bi_3LaTi_3O_{12}$. Experimental, calculated, and difference profiles are shown.

Table 3 gives the final atomic coordinates and ADPs, and Figure 6 shows the Rietveld plot corresponding to this model. These results indicate that a rather satisfactory approximation of the actual micro-distortion can

Table 4. Positional and Thermal Parameters for $Bi_2La_2Ti_3O_{12}$[a]

atom	Wyckoff position	*x*	*y*	*z*	B_{iso}(Å^2)	occ.
Bi(1)	4e	1/2	1/2	0.0668(2)	0.16(9)	0.169(2)
La(1)	4e	1/2	1/2	0.0668(2)	0.16(9)	0.831(2)
Bi(2)	4e	1/2	1/2	0.2129(4)	0.25(5)	0.831(2)
La(2)	4e	1/2	1/2	0.1940(2)	0.25(5)	0.169(2)
Ti(1)	2a	1/2	1/2	1/2	0.48(1)	1
Ti(2)	4e	1/2	1/2	0.3698(1)	0.48(1)	1
O(1)	4c	1/2	0	0	0.64(3)	1
O(2)	4d	1/2	0	1/4	0.64(3)	1
O(3)	4e	1/2	1/2	0.4403(3)	0.64(3)	1
O(4)	4e	1/2	1/2	0.3197(4)	0.64(3)	1
O(5)	8g	1/2	0	0.1166(3)	0.64(3)	1

[a] SG *I*4/*mmm*; $a = 3.8233(3)$ Å, $c = 32.9366(3)$ Å; no. of reflections = 107. Disordered model: $R_p(\%) = 3.6$; $R_{wp}(\%) = 4.9$; $\chi 2 = 8.4$. Ordered model: $R_p(\%) = 4.2$; $R_{wp}(\%) = 5.9$; $\chi 2 = 12.4$.

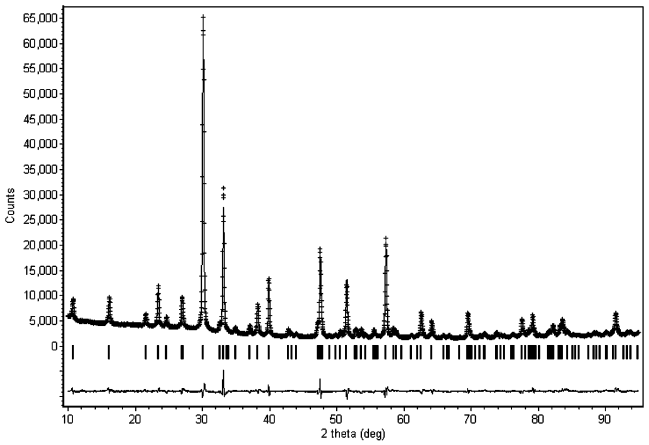

Figure 7. XRD pattern of $Bi_2La_2Ti_3O_{12}$. Experimental, calculated, and difference profiles are shown.

be obtained from powder XRD data. They show that the degree of M/A *cation disorder* is small in BLT1.00 (1.7-(2)% of La in the Bi(2) site), even smaller than that reported by Hervoches et al. (6(1)%[2]). This difference might result from different annealing temperatures (750 °C for 24 h in this study and 1000 °C for 24 h in Hervoches et al.[2]), as Kennedy et al.[10] suggested that the degree of *cation disorder* depends on the annealing temperatures.

3.2.2 BLT2.00. In contrast to that of BLT1.00, the full pattern matching analysis of the XRD pattern of BLT2.00 shows that all diffraction peaks are perfectly interpreted with SG *I*4/*mmm* ($a = 3.8233(3)$ Å and $c = 32.9366(3)$ Å) thereby indicating that the orthorhombic distortion in BLT2.00 is too weak to be characterized by XRD. Therefore the *I*4/*mmm* structural model was refined.

The refinement constraints were practically identical to those applied for BLT1.00, except that isotropic ADPs of oxygens were refined (but constrained to be equivalent). With this model R_{wp} and χ^2 values were lowered to 5.2% and 10.2, respectively. Upon allowing Bi(2) and La(2) to split into two different positions (constraints on isotropic ADPs were kept), R_{wp} and χ^2 values were further reduced significantly, e.g., 4.9% and 8.4, respectively. A similar attempt to split Bi(1) and La(1) into different positions failed. The final atomic coordinates and ADPs are given in Table 4, and Figure 7 shows the Rietveld plot corresponding to this model. This study shows that the degree of M/A *cation disorder* is much more pronounced in BLT2.00 (16.9(2)% of La in the Bi-(2) site) than in BLT1.00, although less than previously reported (18.1(3)% in ref 23 and 21(1)% in ref 2), which is likely a consequence of a lower annealing temperature.[10] In addition, this analysis indicates that La(2) does not occupy the same position as Bi(2) in the $[M_2O_2]^{2+}$ layer, leading to much more regular coordination around the La^{3+} site as already observed for Sr^{2+} in the $Bi_{2-x}Sr_{2+x}Ti_{1-x}Nb_{2+x}O_{12}$ compounds.[2]

3.2.3 Interlayer Mismatch and the Cation Disorder. In a systematic study of bismuth titanate solid solutions with $n = 3$ (considered as crystallizing in the idealized SG *I*4/*mmm*, without *cation disorder*), it was proposed[4] that the size of perovskite-like slabs can be estimated by an empirical formula

$$a = 1.33r_B + 0.6r_A + 2.36 \text{ Å}$$

where r_A and r_B represent the ionic radii of perovskite A- and B-site cations, respectively. With this formula, the *a* parameter of perovskite-like slabs of BTO, $[Bi_2Ti_3O_{10}]^{2-}$, can be estimated to be ~3.89 Å.[4] Therefore, since the unconstrained *a* parameter of $[Bi_2O_2]^{2+}$ layer was considered to be ~3.8 Å, this suggests that the perovskite-like slabs of BTO are under compressive stress.

As already mentioned, the distorted structure of BTO, *B*1*a*1 (No. 7), arises from a commensurate modulation ($q = b^*$) of the orthorhombic average structure (SG *Fmmm*, No. 69) with $a = \sqrt{2} \times a_p$.[3] Therefore, *a* parameters of $[Bi_2O_2]^{2+}$ layer and perovskite-like slabs of *undistorted* $Bi_{4-x}La_xTi_3O_{12}$ compounds can be approximated to be $\sim\sqrt{2} \times 3.8$ and $\sim\sqrt{2} \times (1.33r_B + 0.6r_A + 2.36)$ Å, respectively. Because the ionic radii of Bi^{3+} (1.17 Å) and La^{3+} (1.16 Å) are very close,[24] the substitution of La^{3+} for Bi^{3+} should not affect the size of the perovskite-like slabs, i.e., the mismatch strains in $Bi_{4-x}La_xTi_3O_{12}$ compounds should be very similar. Interestingly, however, these strains are relieved in different ways in BLT1.00 and BLT2.00. In the case of monoclinic BLT1.00, the octahedral tilting is preponderant, whereas in orthorhombic BLT2.00 the size mismatch is relieved by *cation disorder* mainly. Qualitatively, the mismatch relief via *cation disorder* is due to a concomitant effect: La^{3+} and Bi^{3+} tend to occupy different positions in the $[M_2O_2]^{2+}$ layers (and likely also, although not proved, in the perovskite-like slabs), leading to a more regular environment for La^{3+} as can be appreciated from bond lengths in Table 5 (note that results in Table 5 should be taken as approximate, as the actual symmetry of BLT2.00 is orthorhombic). The principal difference between ordered (i.e., $[Bi_2O_2]$ $[La_2Ti_3O_{10}]$) and disordered models (Table 5) arises from the 12-fold coordination of La^{3+} in the $[M_2O_2]^{2+}$ layer, i.e., La(2). With respect to 8-fold Bi(2) with four short Bi(2)−O(2) and four long Bi(2)−O(4) bonds, La(2) moves toward the square "window" of O(4) atoms, forming four additional La(2)−O(5) bonds. This behavior makes La−O bonds in the $[M_2O_2]^{2+}$ layer comparable with those in the perovskite-like slabs (La(1)−O(1), La(1)−O(3), and La(1)−O(5)). It suggests that lanthanum tends to modify its bonding environment in fluorite-like units

(23) Hyatt, N. C.; Hriljac, J. A.; Comyn, T. P. *Mater. Res. Bull.* **2003**, *38*, 837.
(24) Shannon, R. D. *Acta Crystallogr.* **1976**, *A32*, 751.

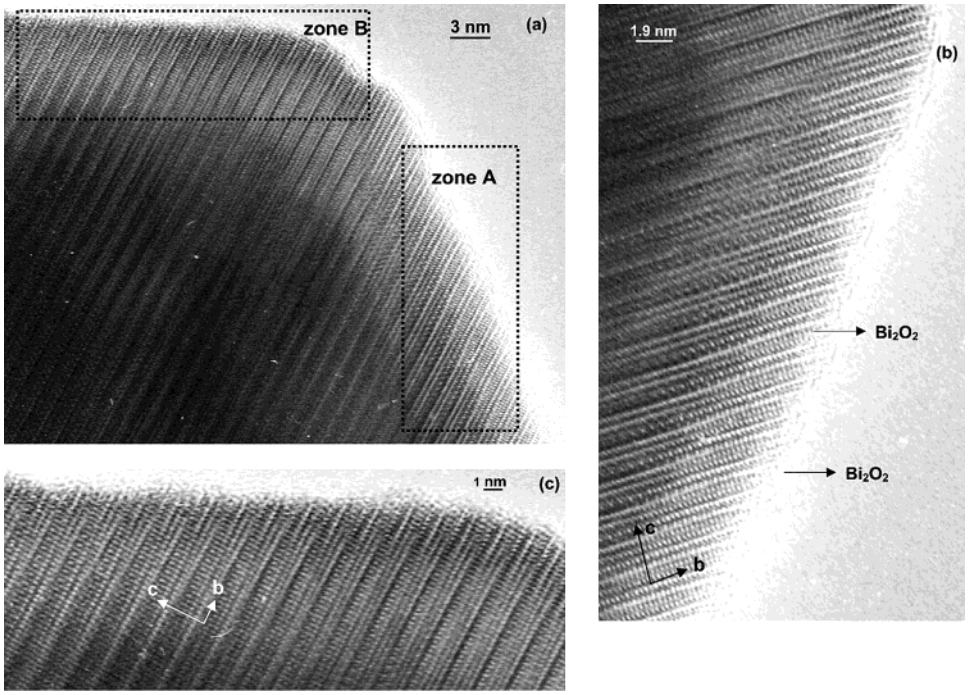

Figure 8. (a) [100] HREM image of $Bi_{3.25}La_{0.75}Ti_3O_{12}$; (b) enlarged image of zone A; (c) enlarged image of zone B.

Table 5. Selected Bond Lengths (Å) for $Bi_2La_2Ti_3O_{12}$

	disordered model	ordered model
[a]La(1)−O(1) × 4	2.915(2)	2.922(3)
[b]La(1)−O(3) × 4	2.714(2)	2.717(2)
[c]La(1)−O(5) × 4	2.519(4)	2.524(4)
Bi(2)−O(2) × 4	2.268(3)	2.298(3)
La(2)−O(2) × 4	2.656(3)	
Bi(2)−O(4) × 4	2.910(6)	2.917(5)
La(2)−O(4) × 4	2.741(3)	
La(2)−O(5) × 4	3.186(5)	
Ti(1)−O(1) × 4	1.912(2)	1.912(3)
Ti(1)−O(3) × 2	1.965(3)	1.944(3)
Ti(2)−O(3)	2.323(4)	2.338(2)
Ti(2)−O(4)	1.649(2)	1.582(4)
Ti(2)−O(5) × 4	1.963(4)	1.958(3)

[a−c] Equivalent to Bi(1)−O(1), Bi(1)−O(3), and Bi(1)−O(5), respectively.

in order to be compatible with the nearest-neighbor perovskite blocks, wherein a simultaneous off-centering of Bi^{3+} is likely and participates in the relief of strain as already proposed.[2]

3.3 HREM Studies. *3.3.1 $Bi_{3.25}La_{0.75}Ti_3O_{12}$ (BLT0.75).* A characteristic HREM image of BLT0.75 along [100] is displayed in Figure 8a. Two zones, A and B, can be observed at the crystal edge showing different stacking sequences. On an expanded scale (Figure 8b and c, respectively), one can note that zone A a priori exhibits an almost regular stacking, while intergrowth defects can be observed in zone B. To understand the origin of contrast differences in these zones, HREM image simulations were performed with the use of crystallographic data inferred from a Rietveld refinement of the structure.[25] Figure 9a shows the calculated through-focus contrast series along [100] with a crystal thickness of 4 nm. In addition Figure 9b demonstrates that contrast differences are not due to thickness effects.

For zone A, the best agreement between calculated and experimental contrasts is obtained at the defocus value of −60 nm (Figure 10), for which the fluorite-like $[Bi_2O_2]^{2+}$ layers are imaged as two bright lines of white dots. The (Bi,La)O planes also show bright contrasts, while TiO_2 planes appear as a dark contrast.

For zone B, intergrowth defects with a thickness of ∼5 nm appear at the crystal edge. To improve the contrast of these defects for further structural study, one part of the experimental HREM image (i.e., Figure 8c) was filtered (Figure 11). From Figure 12, the experimental contrast corresponding to the bulk of crystal (i.e., zone 1 of Figure 11) fits quite well with the calculated contrast of the BLT0.75 structure, i.e., three perovskite-like blocks ($n = 3$) intergrown between two consecutive fluorite-like $[Bi_2O_2]^{2+}$ layers. At this defocus value of −90 nm (with a crystal thickness of 6 nm), the fluorite-like $[Bi_2O_2]^{2+}$ layers appear as two bright lines consisting of white dots, while the perovskite-like slabs ($n = 3$) are imaged as diffused lines with relatively dark contrasts. Note that the thickness of perovskite-like slabs decreases continuously as one moves from the bulk toward the edge of crystal, starting from ∼12 Å (Figure 11, zone 1) to reach ∼8 Å in zone 2, and finally ∼4 Å in zone 3, in such a way that the local structure of the crystal edge (zone 3) is reduced to the thickness of one perovskite block. In addition, the contrast corresponding to $[Bi_2O_2]^{2+}$ layers is strongly modified (see zones 2 and 3 of Figure 11), which suggests that the thickness decrease of perovskite-like slabs is coupled with a structural modification of fluorite-like layers.

Rietveld analyses of XRD data have shown that the M/A *cation disorder* increases with the La content, and that La^{3+} in these $[M_2O_2]^{2+}$ layers tends to adopt a 12-fold environment similar to that in the perovskite-like slabs. Consequently, it is reasonable to suggest that the structural modification of fluorite-like layers characterized in this HREM study arises from the tendency of La^{3+} to form rock-salt-type LaO planes.

According to Boullay et al.'s general structural model for Aurivillius phases,[16] the parent phase $Bi_4Ti_3O_{12}$ (BTO) can be described schematically by an AO−□O_2−

(25) Chu, M.-W. Thesis, University of Nantes, France, 2002.

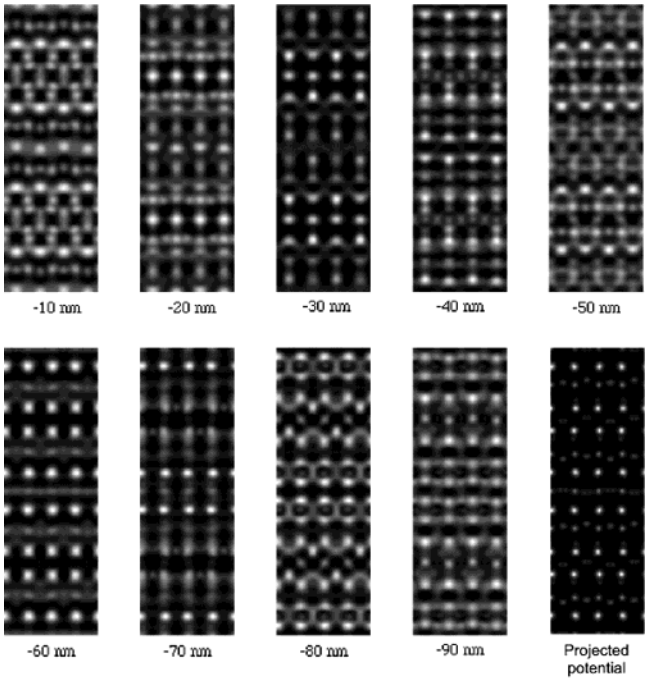

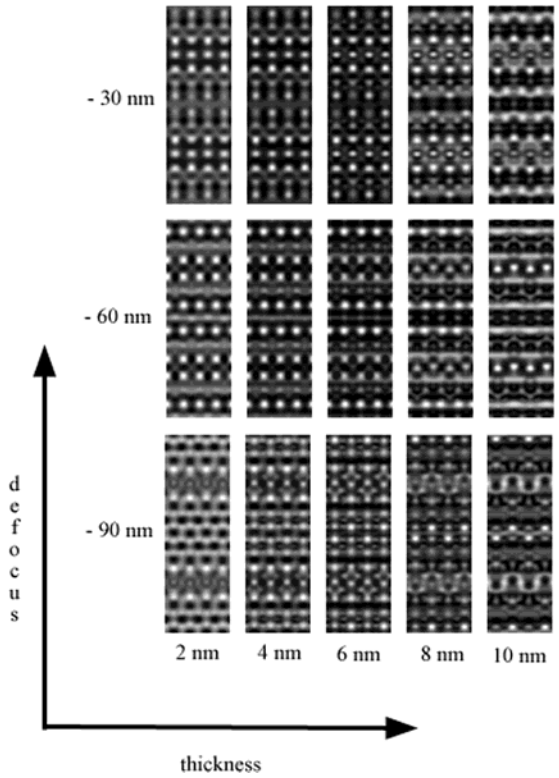

Figure 9. (a) Through-focus series of $Bi_{3.25}La_{0.75}Ti_3O_{12}$ along [100], calculated for a crystal thickness of 4 nm; (b) effect of the thickness on the calculated images for three different defocus values.

$(AO-BO_2)_3$ stacking sequence as illustrated in Figure 13a. Note that octahedral blocks are drawn undistorted for simplicity here, as well as in Figure 13b−e. From Figure 13a, the ABO_3 perovskite structure results from a periodic stacking of AO and BO_2 planes along $[001]_p$ (p, perovskite; i.e., the *c* axis). By analogy, the fluorite-like $[Bi_2O_2]^{2+}$ layer can be described as an $AO-\square O_2-$AO stacking sequence as indicated in Figure 13a, i.e., a sequence wherein the B cation is missing. Therefore,

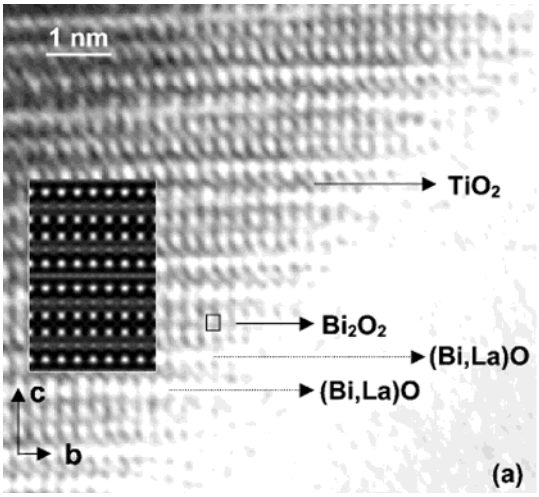

Figure 10. Enlarged experimental image of zone A. The calculated contrast appears as an inset. Calculation parameters: crystal thickness = 4 nm; defocus value = −60 nm.

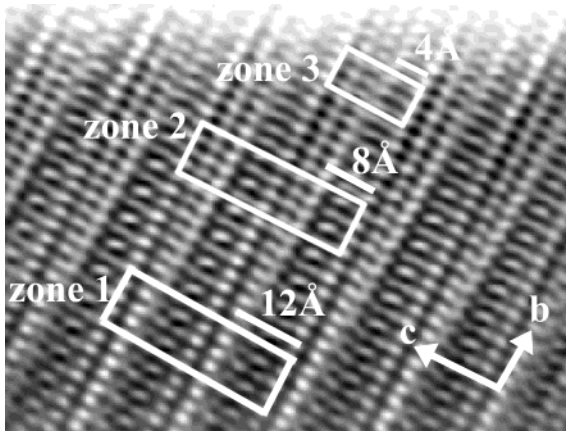

Figure 11. Enlarged and filtered HREM image of part of the crystal in zone B. White rectangles contain the typical contrast for zones 1, 2, and 3.

the $[Bi_2O_2]^{2+}$ layer can be described as a deficient pseudo-perovskite block, as gradually schematized in Figure 13b−e. First, Bi^{3+} in fluorite-like layers is allowed to move into the nearest-neighbor oxygen window in order to form rock-salt-type AO planes (Figure 13b and c). A subsequent in-plane shift of $[^1/_2, ^1/_2, 0]_p$ (p, perovskite; Figure 13d) thus leads to the deficient perovskite $AB_{1-x}\square_xO_3$ (where $\square$ stands for an octahedral B-site vacancy; Figure 13e). Note that this mechanism does not modify the characteristic O_2 plane of fluorite-like layers as can be seen by comparing Figure 13b and e.

Taking this structural description into account, and considering both the enrichment of the surface with La^{3+} and the preference of La^{3+} for a 12-fold coordination, a model can be proposed for the formation of intergrowth defects at the crystal edge of BLT0.75. The substitution of La^{3+} for Bi^{3+} in the $[Bi_2O_2]^{2+}$ layers (schematized in Figure 14a) could induce a $LaO-\square O_2-$LaO stacking sequence via the $[-^1/_2, -^1/_2, 0]_f$ (f, fluorite) in-plane shift (Figure 14b). Further allowing Bi^{3+} to occupy the 6-fold vacant site in the O_2 plane would thereby lead to the $LaBiO_3$ perovskite block displayed in Figure 14c. With the use of this structural model, one can thus suggest that the local structure of the intergrowth defects observed in zone 2 (Figure 11) is a

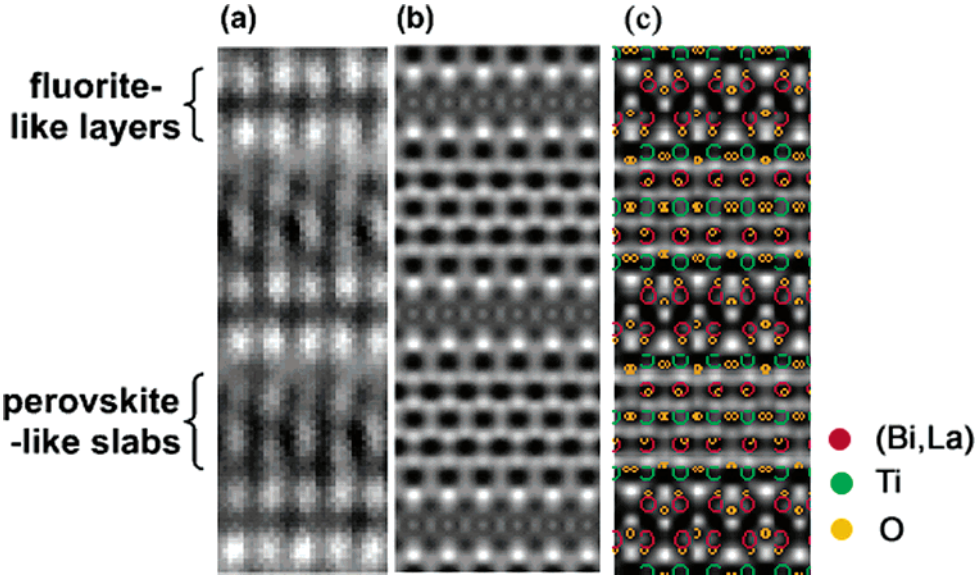

Figure 12. (a) Experimental [100] HREM image of zone 1. (b) Calculated contrast (calculation parameters: crystal thickness = 6 nm, defocus value = −90 nm). (c) Atomic positions are overlaid on the calculated contrast.

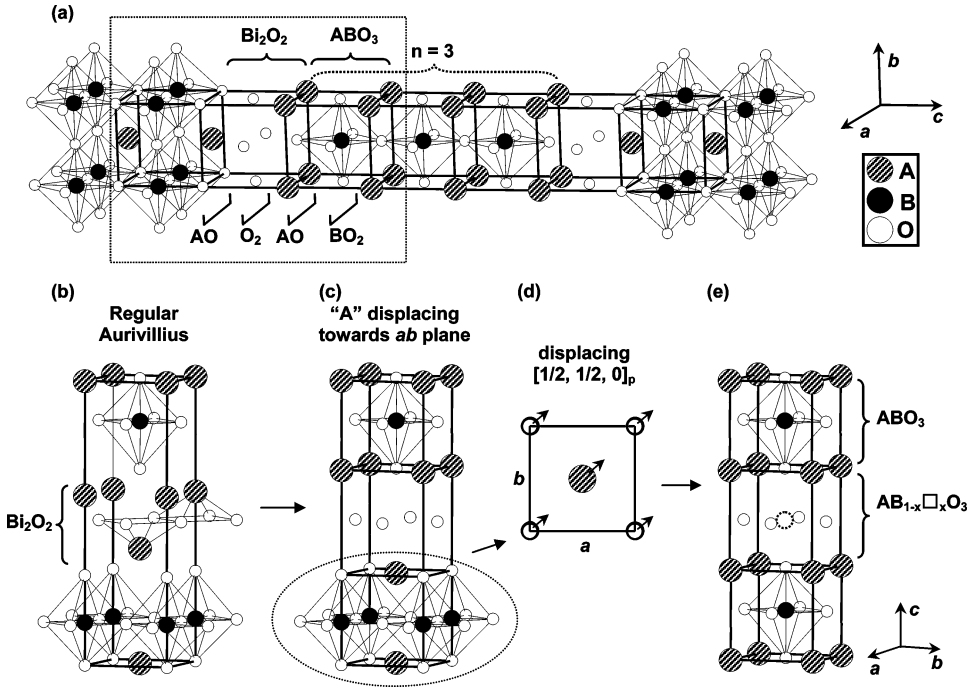

Figure 13. (a) Schematic representation of the AO−□O_2−(AO−BO_2)$_3$ stacking sequence in the n = 3 Aurivillius phase. (b) Regular Aurivillius stacking sequence corresponding to the portion of the schematic structure delimited by a dashed rectangle in (a); from (b) to (c) the Bi^{3+}(A) cations are allowed to move toward the oxygen planes to form rock-salt-type AO planes. (d) In-plane shift of [$^1/_2$, $^1/_2$, 0]$_p$ (p, perovskite) leading to (e) the deficient perovskite $AB_{1-x}\square_xO_3$. Note that all octahedral blocks are drawn in cubic symmetry for simplicity.

quadruple perovskite, $A_4B_4O_{12}$, corresponding to a TiO_2−BiO_2−BiO_2−TiO_2 stacking sequence wherein ordered perovskite-type planes are regularly separated by rock-salt-type AO planes (A = Bi, La) as shown in Figure 15b. The fluorite-like layer and the adjacent perovskite block in zone 1 (Figure 15a) are replaced by a $(Bi_{1-y}La_y)BiO_3$ perovskite slab in zone 2 (Figure 15b). This model agrees with the thickness decrease of perovskite-like slabs (from n = 3 to n = 2) and the experimental contrast modification of fluorite-like layers in zone 2. In addition, a lattice change from *I*-type (body-centered, zone 1) to *P*-type (primitive, zone 2) can be observed in Figure 15a and b, respectively.

To identify the presence of $(Bi_{1-y}La_y)BiO_3$ perovskite slabs, the experimental contrast of zone 2 (Figure 11) was simulated using the crystallographic data of $BaBiO_3$,[26] while replacing Ba^{2+} by La^{3+}. Figure 16 shows the calculated through-focus contrast series along [100] with a crystal thickness of 6 nm using this approximation, and Figure 17 illustrates the best fit between experimental and calculated contrasts. At this defocus value of −50 nm, the rock-salt-type AO planes are related to bright lines consisting of white dots, and the

(26) Pei, S. Y.; Jorgensen, J. D.; Hinks, D. G.; Lightfoot, P.; Zheng, Y.; Richards, D. R.; Dabrowski, B.; Mitchell, A. W. *Mater. Res. Bull.* **1990**, *25*, 1467.

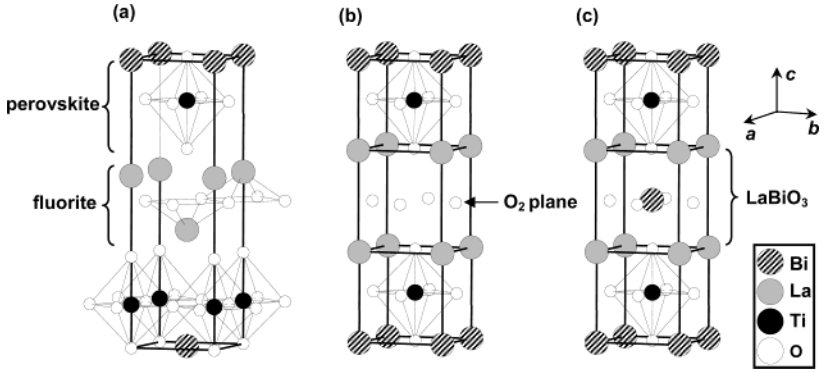

Figure 14. Schematic mechanism of $LaBiO_3$ formation: (a) substitution of La^{3+} for Bi^{3+} in the fluorite-like $[Bi_2O_2]^{2+}$ layer. (b) $LaO-\square O_2-LaO$ stacking sequence via the $[-1/2, -1/2, 0]_f$ (f, fluorite) in-plane shift. (c) Bi^{3+} occupies the 6-fold vacant site leading to a $LaBiO_3$ perovskite block.

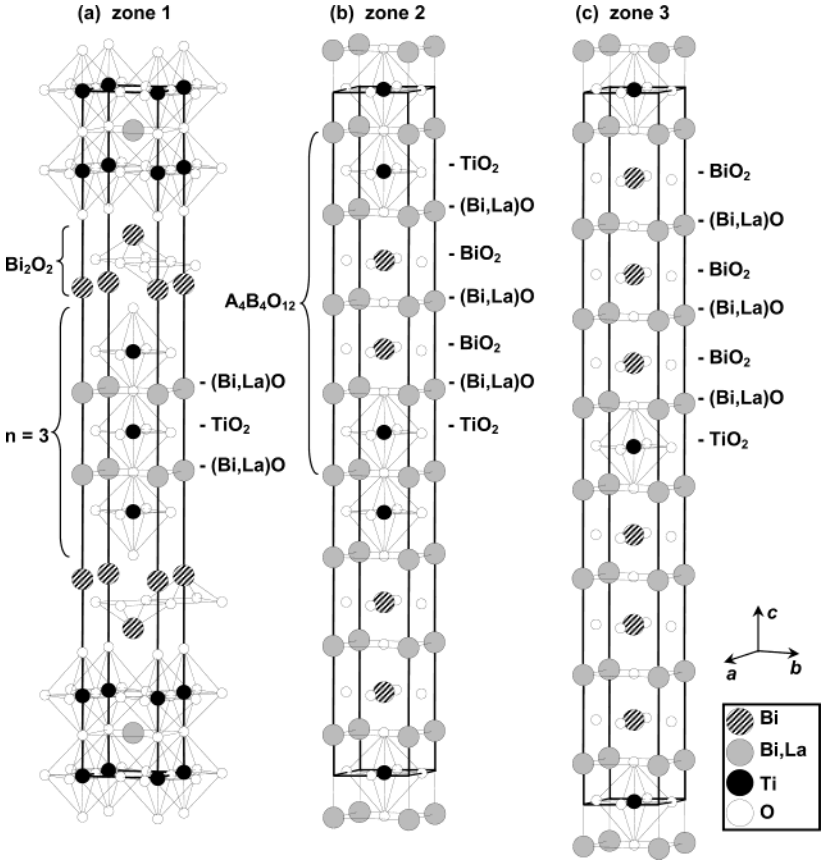

Figure 15. Schematic representation of the structure in the various zones of Figure 11. (a) Zone 1: regular Aurivillius structure of $Bi_{3.25}La_{0.75}Ti_3O_{12}$. (b) Zone 2: $TiO_2-BiO_2-BiO_2-TiO_2$ stacking sequence of planes separated by rock-salt-type (Bi,La)O planes. (c) Zone 3: $BiO_2-BiO_2-BiO_2-TiO_2$ stacking sequence of planes separated by rock-salt-type (Bi,La)O planes.

perovskite-type BiO_2 planes show relatively dark contrasts. Although the actual AO planes are (Bi,La)O rather than LaO, another calculated contrast concerning $(Bi_{1/2}La_{1/2})O$ (with the same crystal thickness and defocus value) exhibits no significant difference with respect to that shown in the insets of Figure 17. The good agreement between experimental and calculated contrasts (Figure 17) suggests that the local structure of zone 2 arises from an ordered intergrowth of two (Bi,La)BiO_3 and two (Bi,La)TiO_3 perovskite blocks along the *c* axis, leading to the quadruple perovskite $(Bi,La)_4Bi_2Ti_2O_{12}$. This latter formula does not take charge balance into account; therefore, since a previous XPS study has shown that La, Bi, and Ti are present as La^{3+}, Bi^{3+}, and Ti^{4+}, respectively,[15] the presence of cation vacancies has to be considered. As cations are more tightly bonded in the 6-fold B sites than in the 12-fold A sites, the creation of cation vacancies in (Bi,La)O planes is much more likely, and the most probable chemical formula would be $(Bi,La)_{3.33}Bi_2Ti_2O_{12}$.

According to the electronic structure study of BTO, Postnikov et al.[27] have indicated that Ti^{4+} in the perovskite blocks next to fluorite-like layers (namely the external ones) shows a strong hybridization with the apical oxygen pointing toward the $[Bi_2O_2]^{2+}$ layers. In contrast, Ti^{4+} in the intermediate perovskite block (i.e.,

(27) Postnikov, A. V.; Bartkowski, St.; Mersch, F.; Neumann, M.; Kurmaev, E. Z.; Cherkashenko, V. M.; Nemnonov, S. N.; Galakhov, V. R. *Phys. Rev. B* **1995**, *52*, 11805.

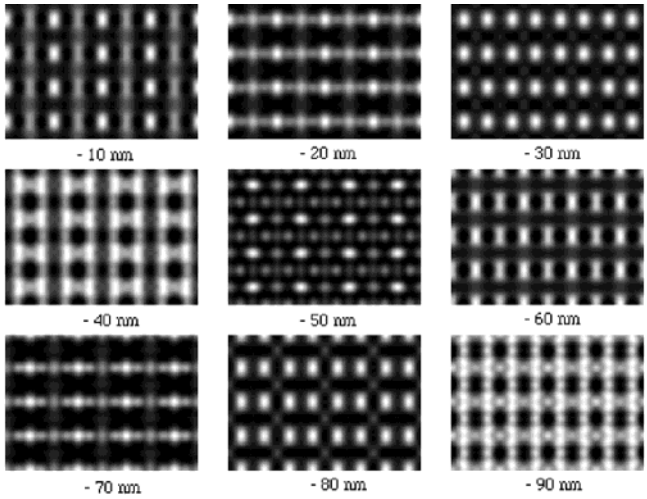

Figure 16. Through-focus series along [100] with a crystal thickness of 6 nm, calculated using the crystallographic data of $BaBiO_3$, while replacing Ba^{2+} by La^{3+}.

sandwiched between two perovskite blocks) does not exhibit this characteristic.[27] Accordingly, Ti^{4+} in the external blocks is relatively covalent in character, whereas Ti^{4+} in the intermediate block is rather ionic. This feature is expected to be also valid for the bulk structure of BLT0.75, as Shimakawa et al.[28] have reported that the electronic structures of bismuth lanthanum titanates are very similar to that of BTO. These characteristics suggest that the substitution of Bi^{3+} for Ti^{4+} would be energetically more difficult in the external perovskite block than in the intermediate block. However, these arguments do not take into account the contribution of elastic energy to the global lattice energy in zones 2 and 3, though it likely plays a predominant role in this outermost region of crystals. As a matter of fact, because of the large difference between their ionic radii, the substitution of Bi^{3+} for Ti^{4+} in the intermediate perovskite block would induce an important mismatch strain on adjacent blocks containing Ti^{4+} (the external blocks), whereas this mismatch strain would take place on one side only for a substitution in an external block. The experimental (Figure 11) and calculated (Figure 17) contrasts based on the structural model of Figure 15b agree with this last argument and indicate clearly that the relief of mismatch strain is a determining factor.

Extending the approach used to model the intergrowth defects in zone 2 to zone 3 (Figure 11), the defective stacking sequence in this zone is (Bi,La)O−BiO_2−(Bi,La)O−BiO_2−(Bi,La)O−BiO_2−(Bi,La)O−

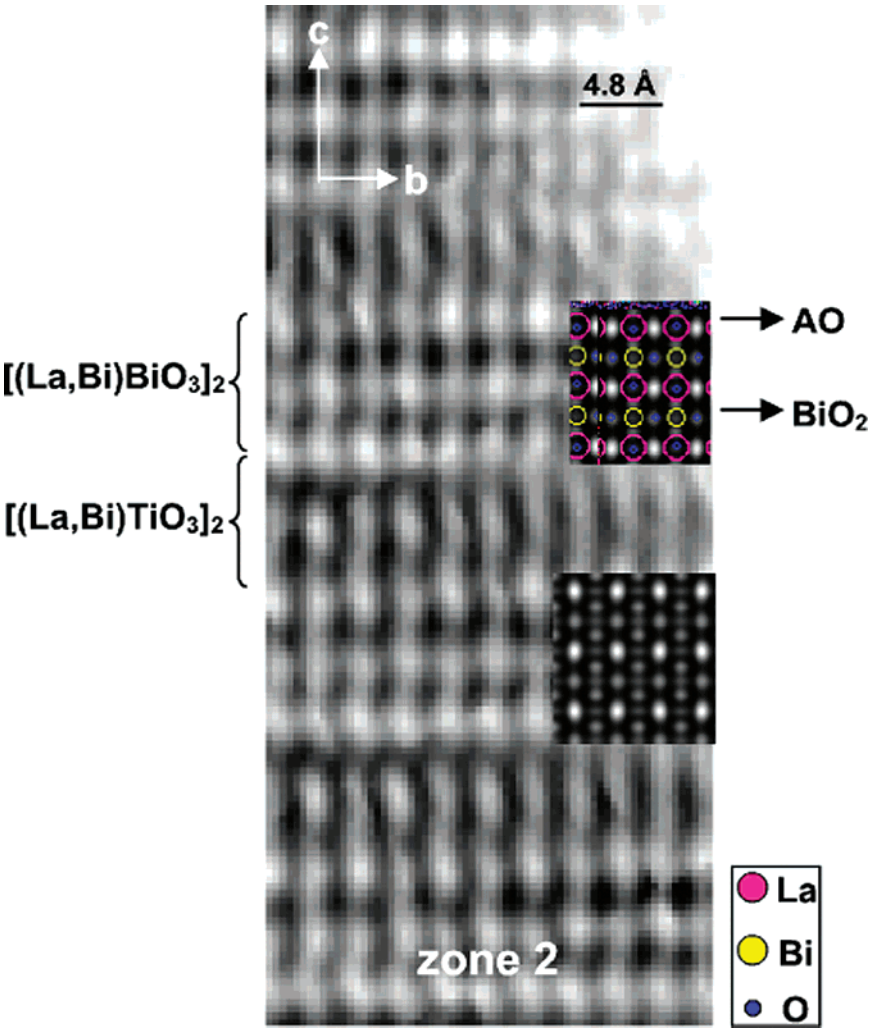

Figure 17. Experimental characteristic contrast of zone 2. The lower inset represents the calculated image (calculation parameters: crystal thickness = 6 nm, defocus value = −50 nm). The calculated image, with atoms overlay, is given in the upper inset.

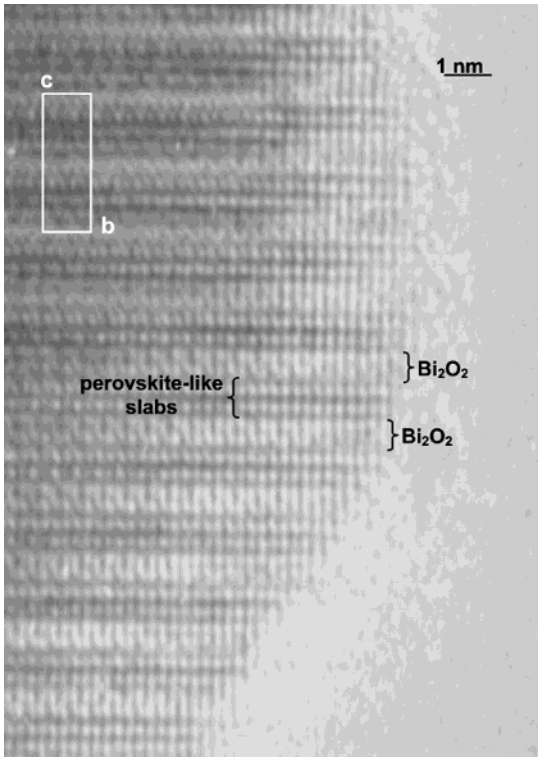

Figure 18. [100] HREM image of $Bi_4Ti_3O_{12}$. TiO_2 planes of perovskite-like slabs appear as dark contrasts, and the rock-salt-type BiO planes appear as two lines of bright spots.

TiO_2 (Figure 15c). With respect to zone 1 (Figure 15a), the stacking sequence in zone 3 arises from the replacement of the external perovskite blocks and fluorite-like layers by three $(Bi,La)BiO_3$ perovskite blocks (Figure 15c), which leads to $(Bi,La)_4Bi_3TiO_{12}$. To maintain the charge neutrality, cation vacancies have to be taken into account, resulting in $(Bi,La)_{3.66}Bi_3TiO_{12}$.

The final formulas, $(Bi,La)_{3.33}Bi_2Ti_2O_{12}$ and $(Bi,La)_{3.66}Bi_3TiO_{12}$, proposed for zones 2 and 3, respectively, indicate a surface enrichment with +3 cations (with respect to Ti^{4+}). For instance, the (Bi,La)/Ti atomic ratio is 2.66 and 6.66 in zones 2 and 3, respectively, and only 1.33 in zone 1 for BLT0.75. The surface enrichment in zone 3 is in fair agreement (within the tolerable range of experimental errors) with the results of quantitative XPS analyses giving (Bi,La)/Ti $\approx$ 8.6 before sputtering.[15]

3.3.2 $Bi_4Ti_3O_{12}$ (BTO) and $Bi_2La_2Ti_3O_{12}$ (BLT2.00). Considering the intergrowth defects in BLT0.75 are suggested to arise from local La^{3+}/Bi^{3+} substitution in fluorite-like layers, it is thereby important to investigate HREM images of BTO (La-free) and BLT2.00 (solid solution member with the largest La content).

Figure 18 shows the HREM image of BTO along [100], and no intergrowth defect can be observed at the crystal edge. The contrast of BTO, calculated according to Hervoches et al.'s crystallographic data,[5] is shown in Figure 19 along with one part of Figure 18 (on an expanded scale). The best agreement between experimental and calculated contrasts is obtained at a crystal thickness of 2 nm and a defocus value of −70 nm. With these conditions, the TiO_2 planes of perovskite-like slabs appear as dark contrasts, and the rock-salt-type BiO planes appear as two lines of bright spots (Figure 19b). In addition, the fluorite-like layers show relatively gray contrasts (Figure 19b). The absence of intergrowth defects in BTO agrees well with the La^{3+}/Bi^{3+} substitution mechanism proposed for BLT0.75, however, it makes the excess of Bi in the sample surface (characterized in quantitative XPS analyses[15]) rather puzzling. This bismuth surface enrichment might result from the presence of an amorphous bismuth oxide layer surrounding the crystal edge (Figure 20), which was also suggested in Nistor et al.'s [29]HREM study of BTO. Note that the thickness of this amorphous layer is almost negligible in the HREM images of BLT0.75 (Figure 8) and BLT2.00 (Figure 21). In addition, intergrowth defects appearing at the crystal edge of BLT2.00 (see the arrows in Figure 21) are similar to those determined in BLT0.75. These characteristics indicate that both the presence of La in fluorite-like layers and the preference of La for a 12-fold coordination are crucial in the formation of intergrowth defects.

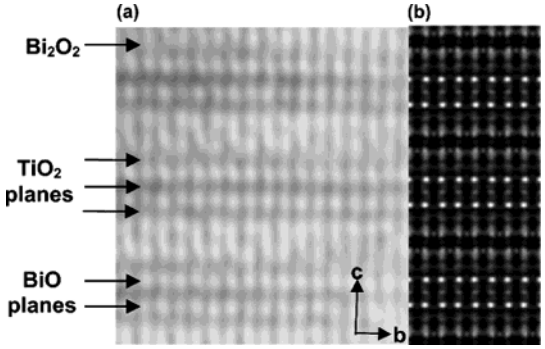

Figure 19. (a) Enlarged [100] HREM image of $Bi_4Ti_3O_{12}$. (b) Calculated image (calculation parameters: crystal thickness = 2 nm, defocus value = −70 nm).

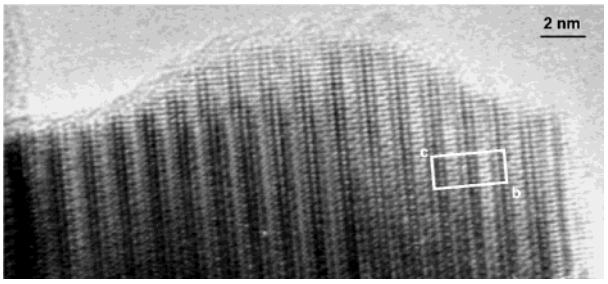

Figure 20. HREM image of a $Bi_4Ti_3O_{12}$ crystal, showing an amorphous bismuth oxide layer surrounding the crystal edge.

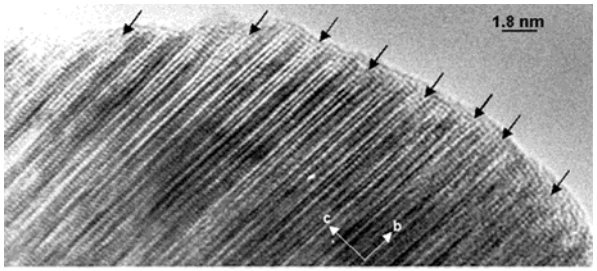

Figure 21. [100] HREM of $Bi_2La_2Ti_3O_{12}$ showing intergrowth defects similar to those observed in $Bi_{3.25}La_{0.75}Ti_3O_{12}$.

(28) Shimakawa, Y.; Kubo, Y.; Tauchi, Y.; Asano, H.; Kamiyama, T.; Izumi, F.; Hiroi, Z. *Appl. Phys. Lett.* **2001**, *79*, 2791.

(29) Nistor, L.; Van Tendeloo, G.; Amelinckx, S. *Phase Trans.* **1996**, *59*, 135.

4. Conclusion

From X-ray and electron diffraction studies it has been shown that the actual bulk structure of $Bi_{4-x}La_xTi_3O_{12}$ ($x \leq 2$) compounds exhibits a small perturbation away from the idealized structure (SG *I*4/*mmm*). In addition to this *lowering of symmetry*, which becomes less important when *x* increases, a disorder of Bi^{3+}/La^{3+} over the M/A sites is observed and it increases when *x* increases. The *lowering of symmetry* and *cation disorder* act simultaneously to relieve the mismatch strain between fluorite-like layers and perovskite slabs.

According to Boullay et al.'s general model for Aurivillius phases,[16] the structure of $Bi_{4-x}La_xTi_3O_{12}$ compounds can be schematized as the ordered intergrowth of $(Bi,La)\square O_3-(Bi,La)TiO_3-(Bi,La)TiO_3-(Bi,La)TiO_3$ blocks with different degrees of La^{3+} substitution, and, consequently, different degrees of *cation disorder*. Because of a significant enrichment of their surface with both Bi and La, structural defects appear at the surface of $Bi_{4-x}La_xTi_3O_{12}$ compounds, whereas they are not observed in the La-free compound BTO. The role of La in the formation of such defects is clearly revealed by the disappearance of the fluorite-like layers. As a matter of fact, because of its preference for the 12-fold coordination, La^{3+} increases the rock-salt-like character of (Bi,La)O planes on both sides of $\square O_2$ planes; a concomitant $[-1/2, -1/2, 0]_f$ (f, fluorite) in-plane shift transforms the square pyramidal cation vacancies into octahedral B sites which can accommodate Bi^{3+}, thus giving rise to a $(Bi,La)BiO_3$ perovskite block. Simultaneously, because of the significant Bi excess with respect to Ti, a substitution of Bi^{3+} for Ti^{4+} occurs in one (and then two) adjacent perovskite block(s). Such intergrowth defects correspond to the formation of A-site cation-deficient perovskite compounds, $(Bi,La)_{3.33}Bi_2Ti_2O_{12}$ and $(Bi,La)_{3.66}Bi_3TiO_{12}$, at the surface of the $Bi_{4-x}La_xTi_3O_{12}$ Aurivillius phases. It has recently been shown that this specific surface structure of BLT crystals behaves as an intrinsic diffusion barrier to Pt; it enables understanding why ferroelectric BLT capacitors with Pt as electrode(s) are almost fatigue-free, whereas Pt−BTO capacitors exhibit fatigue degradation.[30]

CM030341M

(30) Chu, M.-W.; Ganne, M.; Caldes, M. T.; Gautier, E.; Brohan, L. *Phys. Rev. B* **2003**, *68*, 014102.